Applied Clay Science 259 (2024) 107502

Contents lists available at ScienceDirect

Applied Clay Science

journal homepage: www.elsevier.com/locate/clay

Research Paper

Porous metakaolin-based geopolymers for adsorption of Contaminants of Emerging Concern from wastewaters

Serena C. Tarantino [a], Roberta Occhipinti [b,1], Federica Maraschi [a], Michele Zema [c], M. Pia Riccardi [b], Antonella Profumo [a], Michela Sturini [a,*]

[a] Department of Chemistry, University of Pavia, Viale T. Taramelli 12, 27100 Pavia, Italy
[b] Department of Earth and Environmental Sciences, University of Pavia, Via A. Ferrata 9, 27100 Pavia, Italy
[c] Department of Earth and Geoenvironmental Sciences, University of Bari "Aldo Moro", Via E. Orabona 4, 70125 Bari, Italy

ARTICLE INFO

Keywords:
Porous metakaolin-based geopolymers
Clay-based materials
Ofloxacin
Cortisone
Contaminants of Emerging Concern
Wastewaters

ABSTRACT

This research investigates the applicability of metakaolin-based geopolymers in the removal of organic contaminants of emerging concern from polluted water by adsorption. Ofloxacin and cortisone were chosen as model molecules, because of their different chemical properties. For each contaminant, adsorption was first tested on powdered materials with different mesoporosity. The removal of the two drugs was eventually evaluated on macroporous geopolymer monoliths, obtained using commercial olive oil and H_2O_2 solution as pore-forming agents to enhance permeability to liquids and thus favor the absorption process. Finally, a novel ceramic composite diaphragm was prepared and tested. Adsorption experiments demonstrated the larger affinity of all substrates for ofloxacin than for cortisone. Different adsorption mechanisms were observed, monolayer for the antibiotic and cooperative for the steroid, with different adsorption capacities, 29(2) mg g^{-1} and 0.47(2) mg g^{-1}, respectively. The removal efficiencies of the two drugs by the monoliths and by the ceramic composite diaphragm were evaluated and compared. Satisfactory drug recoveries (>99%) were also obtained under realistic conditions, i.e., freshwater, micrograms per liter drug concentration.

1. Introduction

Anthropogenic pressures have significantly changed water availability, quality, and sources (Castiglioni et al., 2020). Due to their high toxicity and severe impact on the safety of human health and aquatic ecosystems, many refractory organic pollutants, including biologically and pharmaceutically active compounds, are causing considerable concern (Castiglioni et al., 2018; Riva et al., 2019). A growing number of Contaminants of Emerging Concern (CECs) are detected in wastewater treatment plant effluents (WWTPs) using analytical screening methods (Gago-Ferrero et al., 2020). Despite the low concentration level, they may cause chronic toxicity to aquatic organisms and accumulation in the ecosystems; moreover, risks to human health cannot be excluded (Riva et al., 2019). Among CECs, antibiotics and endocrine-disrupting substances pose a particular threat, the former stimulating bacterial resistance, and the latter interfering with endocrine functions (Adeel et al., 2017; Kümmerer, 2004).

With increasing amounts of these chemicals being released into our waterways, it is crucial to take action to address this issue, as strongly suggested by the European Union Strategic Approach to Pharmaceuticals in the Environment (European Commission, Directorate-General for Environment, 2019). According to the revised Surface Water Watch List (Gomez Cortes et al., 2022), this approach promotes new strategies for monitoring pharmaceuticals regularly and designing new technologies to reduce their widespread diffusion.

Currently, conventional municipal wastewater treatment plants (WWTPs) are ineffective in eliminating such emerging, highly persistent contaminants, which represent the primary source of drug contamination. To improve WWTP efficiency, several processes have been proposed, conventional (e.g., activated carbon), advanced (e.g., advanced oxidation methods), or combined treatments (Shahid et al., 2021). Removal of pollutants via adsorption is a promising and advantageous option due to its low cost and ease of integration into conventional WWTPs. In addition, no toxic byproducts are generated during treatment, and new generation adsorbent phases make it a more sustainable process. Recently, clay minerals and other materials, such as biochars,

* Corresponding author.
E-mail address: michela.sturini@unipv.it (M. Sturini).
[1] Present address: Department of Biological, Geological and Environmental Sciences, University of Catania, Corso Italia 57, 95129 Catania, Italy

https://doi.org/10.1016/j.clay.2024.107502
Received 14 January 2024; Received in revised form 8 July 2024; Accepted 20 July 2024
Available online 31 July 2024
0169-1317/© 2024 The Authors. Published by Elsevier B.V. This is an open access article under the CC BY-NC-ND license (http://creativecommons.org/licenses/by-nc-nd/4.0/).

biopolymers, metal-organic frameworks, and waste sorbents, have been tested for CEC adsorption (Hossain et al., 2020; Iravani et al., 2022; Mangla et al., 2022; Sophia and Lima, 2018).

Alkali Activated Materials (AAMs) and geopolymers have been intensively studied in the last decades as low-carbon binder alternatives to Portland-based cements (Pacheco-Torgal et al., 2014; Provis and Palomo, 2015; Shi et al., 2019). Moreover, AAMs have many potential applications in the treatment of water and wastewater as adsorbents/ion exchangers, membranes, and filter media (Tan et al., 2020; Papa et al., 2023; Nurlina et al., 2024). Due to mechanical and chemical stability, low cost, and low energy production, AAMs and geopolymers seem advantageous over benchmark standard activated carbon adsorbents, characterized by high energy consumption in manufacturing processes and difficult recovery processes (Liao et al., 2020). Their synthesis allows a variety of different industrial waste to be used as precursors, keeping them in the materials cycle for longer, in line with the circular economy model (Carvalheiras et al., 2023). Another key advantage over the benchmark adsorbent activated carbon is that AAMs can be reused in other applications (e.g., as filler or aggregate in the production of new building materials) after exhaustion due to the strong binding of the pollutants to the geopolymer matrix.

The adsorption of heavy metals and dyes is the result of the porous structure of AAMs and the presence of negative charges on aluminum tetrahedra, as well as of their mechanical stability. Many studies have been carried out on the adsorption of metal ions, including Pb^{2+} (Novais et al., 2016), Cs^{+} (Petlitckaia et al., 2020), Ni^{2+}, Cd^{2+}, Hg^{2+} (Maleki et al., 2019), Cu^{2+} (Duan et al., 2016), and of ammonium (Bai et al., 2017; Sanguanpak et al., 2021). The few studies dealing with organic molecules have mostly focused on the removal of cationic dyes such as methylene blue (En-naji et al., 2023; Novais et al., 2019 and references therein), Crystal Violet (Li et al., 2020) and Basic Yellow 2 (Acisli et al., 2020), as well as anionic Acid Blue 185 (Acisli et al., 2022). Recently, attention has shifted to adsorption of more complex molecules and emerging contaminants, including antibiotics (Sanguanpak et al., 2022), on alkali activated materials. The possibility of using bulk geopolymer-based adsorbents (including porous monoliths, granules, and spheres) rather than powders has gained the interest of the scientific community (see Novais et al., 2020 for a review). In fact, monoliths could be used directly in packed beds, which are safer and easier than nano- or micro-sized powders.

In the present work, the adsorption efficiencies for CECs of metakaolin-based geopolymers were studied on both powdered and centimetre-sized samples under realistic conditions, i.e., micrograms *per* liter drug concentration and freshwater. Ofloxacin (OFL) and cortisone (CORT) were selected as model molecules for several reasons: (i) their widespread use in humans; (ii) their presence in the aquatic compartment; (iii) their largely different physicochemical properties; and (iv) our previous studies on other aluminosilicate sorbents (Belviso et al., 2021; Capsoni et al., 2022; Maraschi et al., 2014; Rivagli et al., 2014; Sturini et al., 2016). Porous geopolymer monoliths were obtained using two different methods, i.e., by chemical foaming technique using hydrogen peroxide, and by emulsion templating method with olive oil. Finally, to design ceramic adsorbents in bulk form that are easy to handle, a composite non-woven fabric ceramic diaphragm was prepared and tested. The drug removal efficiency of the monoliths and the diaphragm were measured and compared with those of the corresponding powders and with powders of geopolymers with the same chemical composition and different porosity.

2. Materials and methods

2.1. Sl-K kaolin clay

The porous geopolymer samples were prepared using Sl-K, an industrial kaolin sourced from the Seilitz kaolin deposits in Germany and provided by Sibelco Italia S.p.a. The chemical composition of Sl-K, as determined by X-ray fluorescence (XRF), is as follows: SiO_2 67.0%, Al_2O_3 31.5%, Fe_2O_3 0.32%, TiO_2 0.24%, CaO 0.12%, MgO 0.23%, K_2O 0.35%. The measured ignition loss of Sl-K is 10.02%, which is lower than the theoretical value for pure kaolinite (13.96%).

Fig. 1a and b show the XRD pattern and FT-IR spectrum of Sl-K, respectively. The XRD pattern in Fig. 1a indicates that the only crystalline phases present are kaolinite and quartz. The FT-IR spectrum (Fig. 1b) is dominated by the bands centered at 1000 cm^{-1} related to T-O stretching in kaolinite and quartz. Furthermore, in the range of 3600 to 3700 cm^{-1}, the spectrum exhibits four intense and well-resolved absorption bands, which correspond to the stretching of groups in kaolinite (Farmer, 1998; Balan et al., 2001).

The relative amount of the two crystalline phases is 73 wt% kaolinite and 27 wt% quartz, as determined by Gasparini et al. (2013), who studied the dehydroxylation kinetics of the sample. Further information on this kaolin clay is reported in other studies (Gasparini et al., 2015; Clausi et al., 2016) where it is used to produce geopolymers. The kaolin powder was heat-treated at 800 °C for 2 h to transform kaolinite into the reactive metakaolinite, hereafter labelled as Sl-MK. The XRD pattern of the heat-treated clay Sl-MK only shows the quartz peaks. The spectrum shows the absence of all stretching bands and those at 910 and 935 cm^{-1} related to Al-O-H. The Si—O peaks have merged into a single broad band centred at 1050 cm^{-1}.

2.2. Other materials

Sodium silicate solution (modulus SiO_2/Na_2O = 2.06 and H_2O = 56.09 wt%) was provided by Ingessil s.r.l. Sodium hydroxide (reagent grade ≥ 98%) was purchased by Sigma Aldrich.

OFL, CORT and acetic acid (AA) were purchased from Merck, high-performance liquid chromatography (HPLC) gradient-grade acetonitrile (ACN) and methanol (MeOH) were by VWR International, H_3PO_4 (85% *w*/w) and water for liquid chromatography (HPLC) by Carlo Erba Reagents.

Working OFL and CORT solutions were prepared daily in tap water collected from the water network of Pavia (pH 7.7, conductivity 278 μS cm^{-1}, see Table S1 in Supplementary Materials).

2.3. Geopolymer synthesis

Sodium silicate solution was modified by adding distilled water and dissolving solid sodium hydroxide to have $Na_2O/H_2O = 14$ (molar ratio) and left to rest one night. Sl-MK was allowed to react with sodium silicate solution to give a final composition characterized by the following molar ratios: SiO_2/Al_2O_3 = 3.7, Al_2O_3/Na_2O = 1.04 and H_2O/solid = 0.33, 0.46 and 0.66 (wt% ratio). Sample labels GpB_33, GpB_46 and GpB_66 reflect water/solid ratios used for the synthesis and are the same used by Clausi et al. (2016). The value of the SiO_2/Al_2O_3 ratio was chosen as it provides the MK-based geopolymers with the highest strength and without formation of crystalline zeolite-type phases, as reported in the literature (Duxson et al., 2005; Fletcher et al., 2005). The different water content of the synthesis produces differences in porosity and median pore radius (in the ranges 20–30% and 4–8 nm, respectively) in the resulting geopolymers (Clausi et al., 2016).

Geopolymer binder samples were prepared by adding Sl-MK powder to the alkaline solutions and mixing for 10 min to form homogenous slurries. Samples were poured into cylindrical PTFE molds and compacted by mechanical vibration for 60 s.

Macroporous monoliths were prepared by using the geopolymer binder slurry GpB_46. The slurry was first mixed with a mechanical mixer for 10 min, then left to rest for 30 min and finally divided into five parts. One part was kept as it is (labelled GpB_46). Another part was used for preparation of the diaphragm composite by coating one side of a non-woven fabric base material evenly with the fresh paste, and then pressing another non-woven fabric sheet on the coated layer and rolling to form the composite diaphragm. Pores forming agents were added to

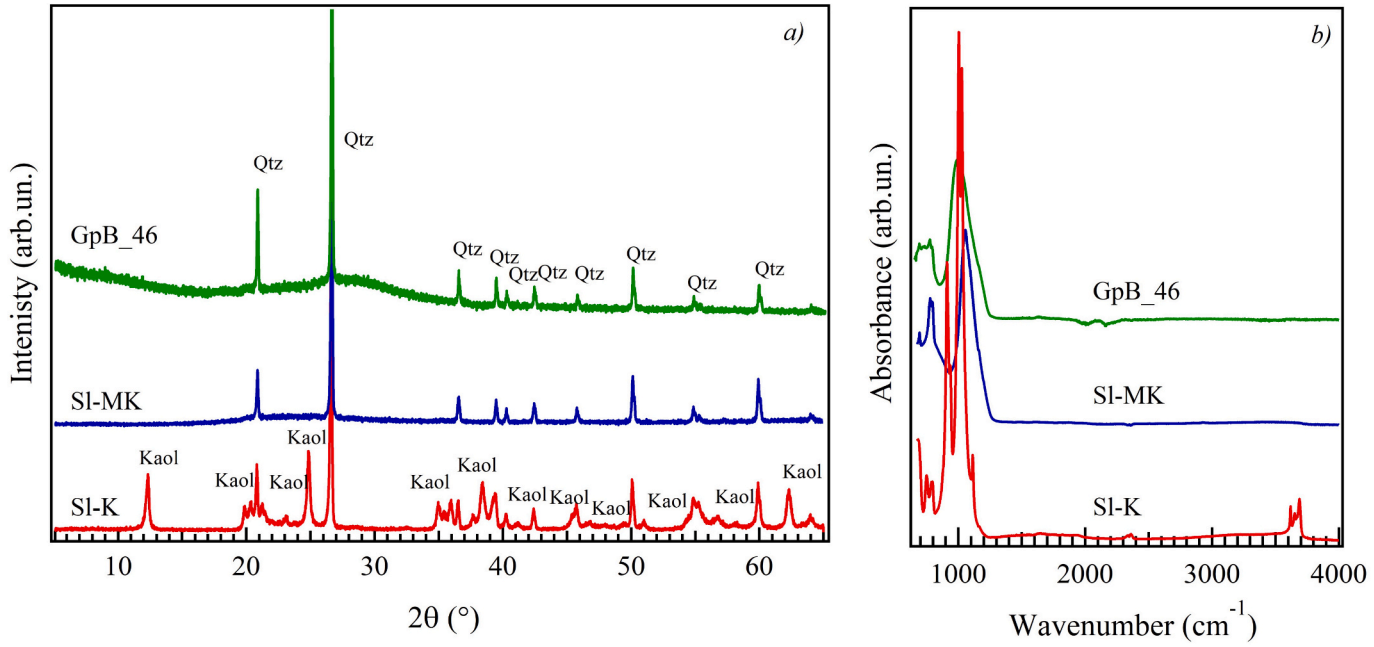

Fig. 1. Characterization of Sl-K kaolin (red), Sl-MK metakaolin (blue) obtained at 800 °C, and geopolymer binder GpB_46 (green). Sample names are reported in the figures. (a) XRD patterns. Main peaks are labelled: Kaol = Kaolinite; Qtz = Quartz; (b) FT-IR spectra. (For interpretation of the references to colour in this figure legend, the reader is referred to the web version of this article.)

the remaining three parts as described below:

1. 25 wt% olive oil. NaOH was also added by considering a saponification coefficient of 0.134. The resulting sample is labelled GpB_46_O;
2. 1 wt% hydrogen peroxide solution (30% Sigma Aldrich), as described by Ducman and Korat (2016). The resulting sample is labelled GpB_46_HP1;
3. 6 wt% hydrogen peroxide solution. The resulting sample is labelled GpB_46_HP3.

The resulting slurries were mixed again for 10 min, poured into cylindrical molds, and cured at 52 °C for 19 h in sealed vessels to ensure 100% Relative Humidity before being demolded.

Such curing conditions were chosen as they can produce metakaolin-based geopolymers with high strength and low shrinkage (Gasparini et al., 2015).

2.4. Geopolymer characterization

X-ray powder diffraction (XRPD) analyses were carried out on all samples by using a Malvern Panalytical X'Pert3 X-ray diffractometer, equipped with a Cu anticathode operating at 40 kV and 40 mA, in the range 2°-65° 2θ. XRPD patterns of all samples are similar showing a broad hump between 20° and 35° 2θ, typical of the amorphous phase of geopolymers and the presence of quartz, derived from the metakaolin. The XRPD pattern of sample GpB_46 is shown in Fig. 1a as a representative for all samples, and compared with the pattern of Sl-MK. No peaks resulting from the presence of new crystalline phases, such as zeolite phases, were detected in any of the patterns apart from GpB_46_HP3, which show peaks due to trona, $Na_3(CO_3)(HCO_3)\cdot 2(H_2O)$. The formation of sodium carbonate formation may be due to an excess of Na cations that are mobile within the pore network. As water evaporates, they are brought to the surface where they can react with atmospheric CO_2. Diffraction patterns of all geopolymer samples are available in Fig. S1 in Supplementary Materials.

Apparent densities of monoliths were measured by a ULTRAPYC 1200e gas ultrapycnometer 244 (Quantachrome Instruments, USA). Measurements were carried out in a sample chamber of 48.1 cm^3 and by using nitrogen as pycnometric gas. Three different roughly cubic specimens (1.4 × 1.4 × 1.4 cm^3), dried at 80 °C for 24 h, were measured for each sample composition. For each specimen, density was obtained by averaging six measurements. Data accuracy is < ±0.02% and reproducibility is < ±0.01%. Stainless-steel spheres were used for instrument calibration.

Apparent density (D_{app}) is defined as the ratio of sample weight to its apparent volume V_{av}, which excludes open pores, but includes closed pores, as measured by the pycnometer. Nominal density (D_{nom}) is instead based on the geometrical volume V_{geo}, i.e., that calculated from the measured sample linear dimensions. Sample effective porosity φ was evaluated by $(1 - D_{app}/D_{nom}) \times 100$. D_{app}, D_{nom} and porosity of geopolymer monoliths are reported in Table 1.

The measured density values of geopolymers of this work are around 2 g/cm^3, in agreement with data previously reported in the literature for geopolymers of similar Si/Al ratio (Duxson et al., 2005; Rovnanik, 2010). The density of GpB_46_O is slightly lower, probably because not all the pores are interconnected, and the lower weight of the isolated voids within the matrix reduces the mass/volume ratio.

Samples were analyzed by using optical and electron scanning microscopes. Pictures of massive samples and optical microscope images are reported in Fig. S2. Microtextural investigations were performed using a stereomicroscope Olympus SZ61. A Field Emission Scanning Electron Microscope TESCAN Mira 3 XMU-series. Analyses of the morphological features were performed on fracture surfaces of the specimens, obtained by placing thin splinters of material directly on the stab. Samples were covered by 5 nm carbon coating before being

Table 1
Density and effective porosity of porous alkali activated monoliths. Errors reported in table are twice the standard deviations of the six measurements carried out on each sample.

Sample name	D_{nom} (g/cm^3)	D_{app} (g/cm^3)	Porosity φ (%)
GpB_46_O	0.9(1)	1.8(1)	50
GpB_46_HP1	1.3(1)	2.2(1)	41
GpB_46_HP3	0.5(1)	2.3(1)	78

investigated to prevent charge built-up on the electrically insulating sample surface. Images were collected using secondary electrons (SE).

2.5. Adsorption experiments

2.5.1. Drug adsorption tests

50 mg of each material was suspended in tap water samples (10 mL) containing OFL and CORT, each separately. Two different concentrations were investigated, i.e., 10 mg L^{-1}, 50 μg L^{-1}. A small amount of diluted acidic and alkaline solutions (HCl ≈ 1 M and NaOH ≈1 M) was added to adjust the pH. The suspensions were gently shaken on a rocker overnight at room temperature. They were centrifuged, and the supernatants were withdrawn, filtered, and analyzed by UV–Vis and HPLC systems to determine the residual drug concentrations in the solution.

The drug removal efficiency (R %) was calculated from Eq. 1:

$$R\% = \frac{(C_0 - C_e)}{C_0}\, x\, 100 \quad (1)$$

where C_0 is the initial drug concentration, C_e is the concentration after stirring overnight.

2.5.2. Isotherm study

A batch equilibration method was used to describe the adsorption isotherms of the two drugs on powders of geopolymer samples to evaluate the maximum drug uptake and the relation between the amount of adsorbed drug (q_e) and its concentration in the solution (C_e) at equilibrium (Foo and Hameed, 2010). 50 mg of each material were weighed into flasks and mixed with 10 mL of tap water samples containing increasing amounts of each drug, depending on their water solubility. The flasks were gently shaken on a rocker for 24 h at room temperature (20 ± 1 °C) to ensure equilibration. The suspensions were filtered through a 0.22 μm nylon membrane filter and analyzed by UV-mini and HPLC-UV to determine OFL and CORT concentration at equilibrium (C_e).

The amount of drug adsorbed (q_e) was calculated from Eq. 2:

$$q_e = \frac{(C_0 - C_e) \times V}{M} \quad (2)$$

where C_0 is the initial drug concentration, C_e the concentration in solution at equilibrium, V the volume of the solution (L) and M the amount of the sorbent (g).

All experiments were performed in duplicate with good reproducibility (RSD ≤10%).

The isotherm parameters were determined by OriginPro, Version 2019b (OriginLab Corporation, Northampton, MA, USA).

2.6. Analytical measurements

UV–Vis and HPLC systems with different sensitivity and analysis modes were used according to the type of analyte and its concentration, as previously reported (Capsoni et al., 2022).

OFL at mg L^{-1} was quantified by a UV–Vis spectrophotometer (UVmini-1240, Shimadzu Corporation) (λ = 287 nm, calibration range 1–10 mg L^{-1}, $R^2 > 0.9988$, quantification limit 0.8 mg L^{-1}). OFL at μg L^{-1} was determined by an HPLC system consisting of a pump Series 200 (Perkin Elmer, Milano, Italy) equipped with a vacuum degasser and a programmable fluorescence detector (FD) setting the fluorescence excitation/emission wavelengths at 280 and 450 nm (50 μL injection sample volume, Ascentis RPAmide column 250 × 4.6 mm, 5 μm coupled with a similar guard-column, mobile phase 25 mM H_3PO_4–ACN 85:15, flow rate of 1 mL min^{-1}; calibration range 1 and 20 μg L^{-1}, $R^2 > 0.9988$, quantification limit was 0.9 μg L^{-1}).

For CORT measurements at mg L^{-1}, an HPLC-UV Shimadzu (Shimadzu Corporation, Milano, Italy) system, consisting of a LC-20 AT solvent delivery module equipped with a DGU-20 A3 degasser and interfaced with a SPD-20A UV detector, was used (λ_{max} 238 nm, injection sample volume 20 μL, 250 × 4.6 mm, 5 μm GraceSmart RP18 column coupled with a similar guard-column, isocratic elution H_2O–ACN 70:30, flow rate was 1.0 mL min^{-1}; calibration range 1–10 mg L^{-1}, $R^2 > 0.9996$, quantification limit was 0.3 mg L^{-1}) (Pretali et al., 2021).

An Agilent (Cernusco sul Naviglio, Italy) HPLC 1260 Infinity apparatus coupled with an Agilent 6460C ESI-MS/MS spectrometer was used for CORT analyses at μg L^{-1} (injection sample volume 5 μL, Agilent 120 EC-C18 Poroshell column 50 × 3 mm, 2.7 μm with a similar guard-column; mobile phases ultrapure H_2O 0.1% *v*/v acetic acid (A) – MeOH 0.1% v/v acetic acid (B), linear gradient from 40% to 84% B in 12 min, followed by 8 min column re-equilibration, 0.6 mL min^{-1} flow rate, column temperature 50 ± 1 °C).

The MS/MS system consisted of a triple quadrupole with electrospray ionization (ESI) source operating in negative mode (precursor ion [M + AcO] − adduct). The source parameters were: drying gas temperature 300 °C (N_2); drying gas flow 5 L min^{-1} (N_2); nebulizer 45 psi; sheath gas temperature 250 °C; sheath gas flow 11 L min^{-1}; capillary voltage 3500 V (positive mode) and 3000 V (negative mode); nozzle voltage 500 V positive, 0 V negative; electron multiplier voltage (EMV) 0 V for both polarities; cell accelerator voltage (CAV) 1 V. The multiple reaction monitoring (MRM) conditions for the target analyte are reported in (Pretali et al., 2021). The instrumental quantification limit was 0.6 μg L^{-1}. MassHunter software from Agilent was used for data processing.

3. Results and discussion

In the present work, the potential use of geopolymers as novel sorbents for the removal of OFL and CORT from wastewater was evaluated. Affinities of these materials towards the selected model drugs were tested on both powders and bulk specimens. Adsorption efficiencies were evaluated also under relevant realistic conditions (freshwater; μg L^{-1} drugs).

3.1. Microstructural features of geopolymers

Differences in the morphology of the geopolymer samples are hereafter analyzed based on high-resolution SEM images at different magnifications. At low magnifications (Fig. 2, left panel), matrix homogeneity and the presence of porosity are taken into account, and in particular, the abundance, shape, dimension, and arrangement of the pores were evaluated.

Analyses at higher magnifications (10kx, Fig. 2, right panel) allow to evaluate fine details of the aluminous gel and its degree of development. Moreover, they clearly display the differences in the microstructural features and texture of the samples and hence allow to evaluate the effect of the foaming agents on the geopolymer binding matrix.

At 150x, GpB_46 shows a homogeneous and dense texture, spherical voids of 50–70 μm in size are evident, probably due to air bubbles trapped in the gel during the synthesis. They contribute to the total porosity but are not connected but isolated one from the other.

The matrix of the GpB_46 sample, observed at 10kx magnification (Fig. 2b), appears to be characterized by a high homogeneity with a fairly rough surface, given by the precipitated gel particles that are linked to each other in an ordered arrangement forming a binding tissue that appears continuous even at large magnifications.

New crystalline phases are not present, but relicts of metakaolinite, recognizable by the typical lamellar structures, can be seen. However, they are completely incorporated in the matrix.

The GpB_46_O sample has a high porosity, as can be seen from Fig. 2c. The pore size is fairly heterogeneous, ranging from 150 μm to 10 μm. The photo allows observing that there is a certain degree of effective porosity, as the largest pores show interconnection. At higher magnification (Fig. 2d), the GpB_46_O sample matrix is very compact. The particles are all organized to form parallel structures, as is evident from

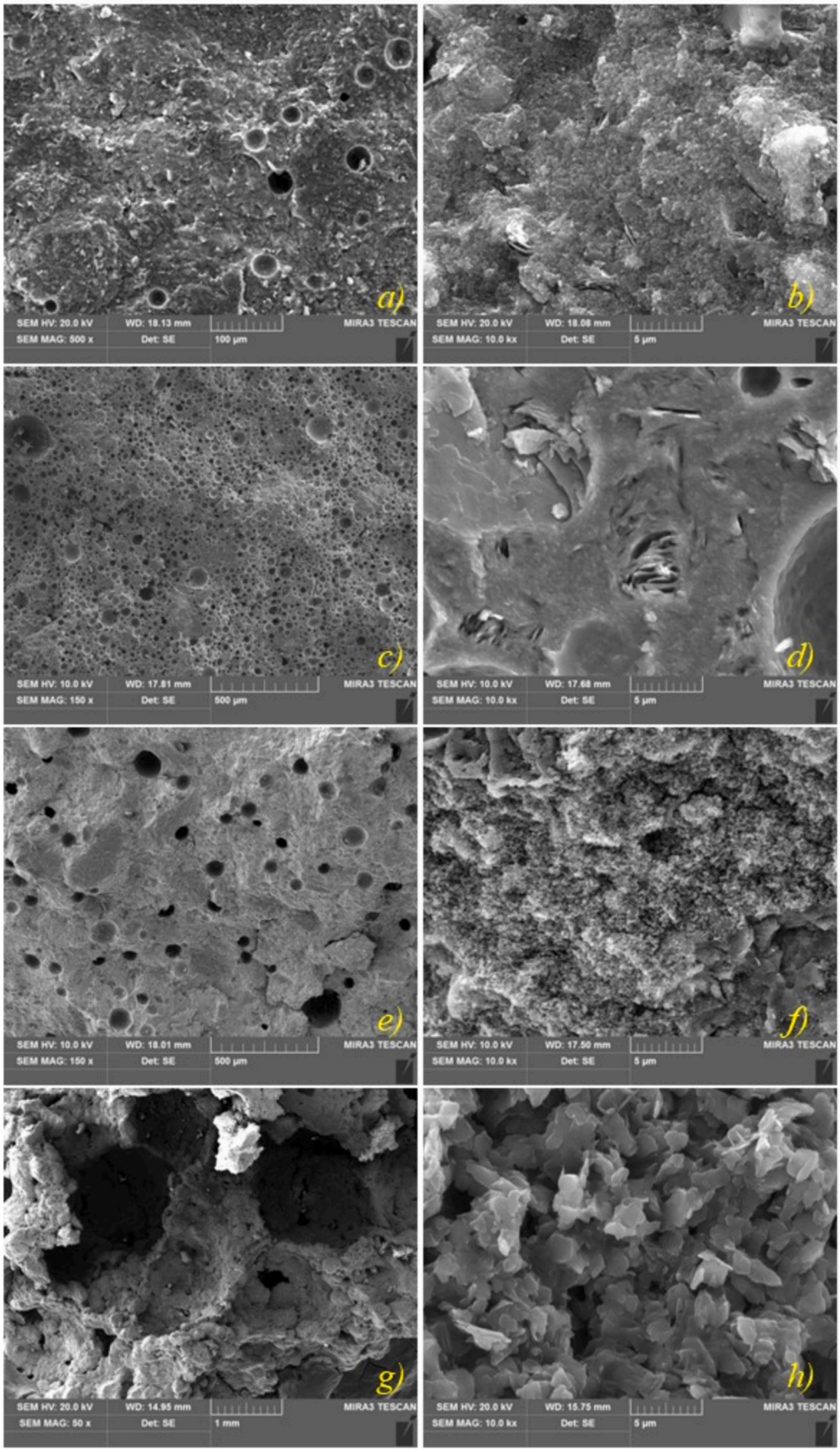

Fig. 2. FESEM micrographs of geopolymer samples at different magnifications. Each row refers to one sample. a), b): GpB_46; c), d): GpB_46_O; e), f): GpB_46_HP1; g), h): GpB_46_HP3. Scale bar, magnification (MAG), acceleration voltage (HV) and working distance (WD) are shown in each image.

the detail in the upper left, and no porosity is evident at that scale. Moreover, relicts of metakaolinite, incorporated into the matrix, can be seen.

The GpB_46_HP1 sample has a uniform pore shape and size, ranging from 50 to 100 μm (Fig. 2e). In this case, the pores appear uniformly distributed but not in connection with each other, if we exclude the microfractures due to the preparation operations. In the 10kx magnification image (Fig. 2f), the matrix is coarser than that of GpB_46_O, slightly loose, and shows some fine porosity in some areas (top left and bottom right), the particles tend to be more compact and create parallel layers.

In sample GpB_46_HP3, the higher amount of hydrogen peroxide resulted in pores of 1 to 2 mm (Fig. 2g), still well distributed in the material. This behavior is due to the pore coalescence, which clearly leads to an increase in pores size. To highlight the pore diameter of this sample, a lower magnification was required (50x, compared to 150x used for GpB_46_O and GpB_46_HP1 and 500x for GpB_46). In Fig. 2h the coarse grain of the matrix and an incipient crystallization process can be observed. The degree of anisotropy is high, and the matrix has a relatively loose structure.

3.2. Drugs adsorption on powdered geopolymer

3.2.1. Preparatory adsorption tests

Preparatory experiments were carried out to evaluate the feasibility of the sorption process of the drugs at two different drug concentrations (10 mg L^{-1}, 50 μg L^{-1}) under environmental conditions. For this purpose, tap water was chosen as the solvent because its composition is constant over time and very similar to freshwater (see Table S1). In this way, the adsorption properties of metakaolin-based geopolymers were tested in the presence of the matrix macro-constituents (see Table S1), which are also the predominant species in most freshwater systems (Syeed et al., 2023), and can affect the drug uptake (Rivagli et al., 2014; Chang et al., 2022). Likewise, we investigated a pH range, from 4.0 to 9.0, that includes the pH values found in many natural water bodies, falling between pH 6.5 and 8.0.

The adsorbent amount was chosen based on our previous experimental evidence on clay minerals, such as kaolinite, montmorillonite (Rivagli et al., 2014), and sepiolite (Sturini et al., 2016) used for FQs adsorption. The high adsorption capacities of such materials, ranging from 9 to over 200 mg g^{-1}, and the recent literature regarding contaminants adsorption on geopolymers (Salimkhani et al., 2021) prompted us to use small amounts of metakaolin-based geopolymers, also avoiding an excess of waste. Finally, we considered stirring each suspension overnight for operative reasons despite the fast equilibration time attained for kaolinite in our previous study (Rivagli et al., 2014).

Fig. 3a shows the OFL removal efficiency profiles of GpB_33, GpB_46, and GpB_66 powders as a function of pH. The adsorption efficiency increases significantly with the decrease in pH,from 20 to 30% at pH > 8 to 80–90% below pH 6.5, independently of the different water/solid ratios used to prepare the samples and, in turn, independently of differences in their porosity.

Quite similarly, the pulverized geopolymers GpB_46_O, GpB_46_HP1, and GpB_46_HP3, guarantee an OFL removal ≥90% below pH 6.5. However, it can be seen from Fig. 3b that at pH values above 6.5, the OFL adsorption decreases dramatically for GpB_46_HP3 and more gradually for GpB_46_O.

Differently, CORT removal is around 16–19% and it does not change in the pH range from 4.0 to 9.0 for all the investigated materials (Fig. 4a). Adsorption of CORT by the samples obtained with the use of pore-forming agents is not significantly different and varies between 7 and 14% (Fig. 4b).

Such different trends may be related to the different chemical properties of the selected molecules and, consequently, to the different adsorption interactions between the drug and the surface of the geopolymer samples.

The experimentally determined pHpzc value, around 8, for GpB_46 (Fig. S3 in Supplementary Material) implies that its surface is positively charged below pH 8, almost uncharged around pH 8, and negatively charged in alkaline solution. According to the dissociation constants pK_{a1} (5.98) and pK_{a2} (8.00) of the antibiotic (Babić et al., 2007; Van Doorslaer et al., 2014), the relevant OFL species at environmental conditions are the positively charged (OFL^{+}) and the zwitterionic ($OFL^{\pm}$) species. Thus, as previously reported (Rivagli et al., 2014), we may assume that cation exchange between the exchangeable cations of the geopolymer - particularly the excess of sodium cations incorporated during the synthesis and mobile within the pore network- and the protonated amine group of the piperazine moiety of the antibiotic is the predominant adsorption mechanism at pH solution below pK_{a1}. For pH solution between pKa_1 and pKa_2, the removal efficiency of the geopolymer gradually decreases, suggesting that the positively charged amine group of the antibiotic may still contribute to the adsorption, even though the antibiotic is in the zwitterionic form. However, we do not exclude the presence of hydrogen bonding interactions between the ionized carboxylic group and the positively charged surface of the geopolymer. At pH solution >8, OFL and the GpB_46 surface gradually become negatively charged, and electrostatic repulsions occur between the negatively charged carboxylic group in the quinolone moiety (OFL^{-})

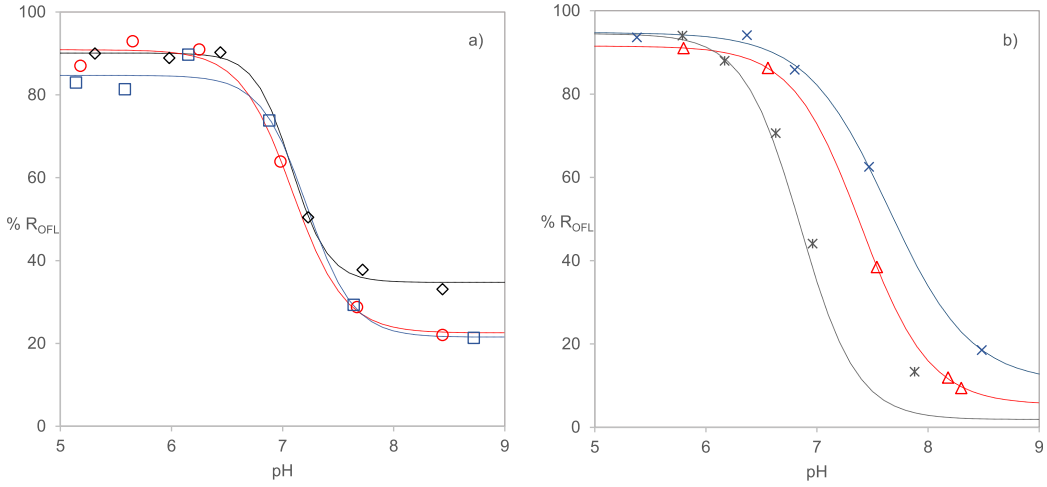

Fig. 3. OFL removal efficiency of: (a) GpB_33 (◊), GpB_46 (○) and GpB_66 (□); (b) GpB_46_O (×), GpB_46_HP1 (△), and GpB_46_HP3 (*) (Experimental conditions: 50 mg powder, 10 mg L^{-1} OFL, 10 mL tap water).

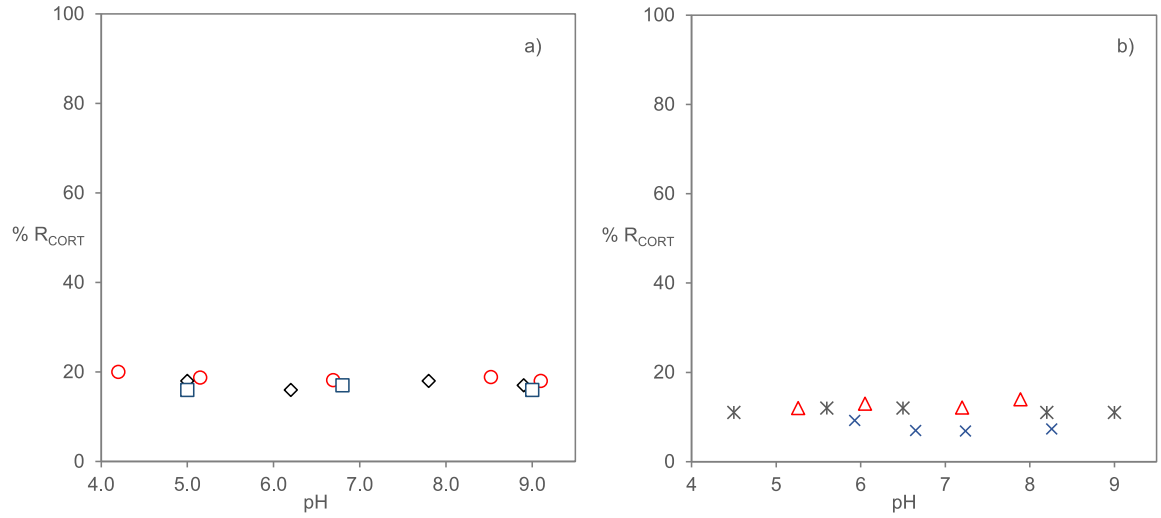

Fig. 4. CORT removal efficiency of: (a) GpB_33 (◇), GpB_46 (○), and GpB_66 (□), and (b) GpB_46_O (×), GpB_46_HP1 (△), and GpB_46_HP3 (*) (Experimental conditions: 50 mg powder, 10 mg L^{-1} CORT, 10 mL tap water).

and the negatively charged surface of the geopolymer. FTIR-ATR spectrum of GpB_46 enriched with OFL may support these assumptions (Fig. S4) (Sahoo et al., 2011). On the contrary, CORT is a hydrophobic and non-polar molecule; its behavior agrees with literature data on the adsorption of hydrophobic compounds by modified clays (Barreca et al., 2014) through non-polar and van der Waals interactions.

Finally, GpB_46 powder was tested to remove OFL and CORT, each separately, from tap water spiked at concentration of μg per liter (50 μg L^{-1}). After stirring overnight at room temperature, the GpB_46 powder was separated, and the residual amounts of OFL and CORT in the solutions were determined by HPLC-FD and HPLC-MS/MS, respectively. Quantitative adsorption (residual amount in solution < instrumental detection limits) of both drugs was observed, suggesting the potential use of the geopolymer for environmental applications.

3.2.2. Adsorption isotherms

Based on the results shown in Fig. 2a and b, and Fig. 3a and b, the determinations of the adsorption isotherms, aimed at highlighting the maximum drug uptake and the type of adsorption at equilibrium, were carried out on powders of GpB_46 at pH around 6.

Fig. 5a and b show the experimental adsorption profiles of OFL and CORT.

The two most commonly used models, i.e., Freundlich and Langmuir, and the sigmoidal model, were used to fit the experimental data. The Freundlich model describes the non-ideal sorption on the heterogeneous surface and is expressed by the following equation:

$$q_e = K_F C_e^{1/n} \tag{3}$$

where K_F is the empirical constant indicative of sorption capacity, and n is the empirical parameter representing the heterogeneity of site energies.

The Langmuir model assumes that the sorption process occurs in a monolayer that covers the surface of the material:

$$q_e = \frac{q_m K_L C_e}{1 + K_L C_e} \tag{4}$$

where K_L is the Langmuir constant and q_m the maximum uptake.

The sigmoidal model describes cooperative adsorption and is expressed by the equation:

$$q_e = \frac{q_m}{1 + e^{-A(C_e - F)}} \tag{5}$$

where q_m max is the maximum amount of molecules adsorbed, A is a coefficient indicating the efficiency of the adsorption mechanism, and F represents the inflection point.

As shown in Fig. 5a and b, OFL and CORT show very different behaviors. The Langmuir model provides the best fit for OFL data, while the sigmoidal model better describes the CORT profile. The correlation coefficients are 0.9916 and 0.9892, respectively, as reported in Table 2.

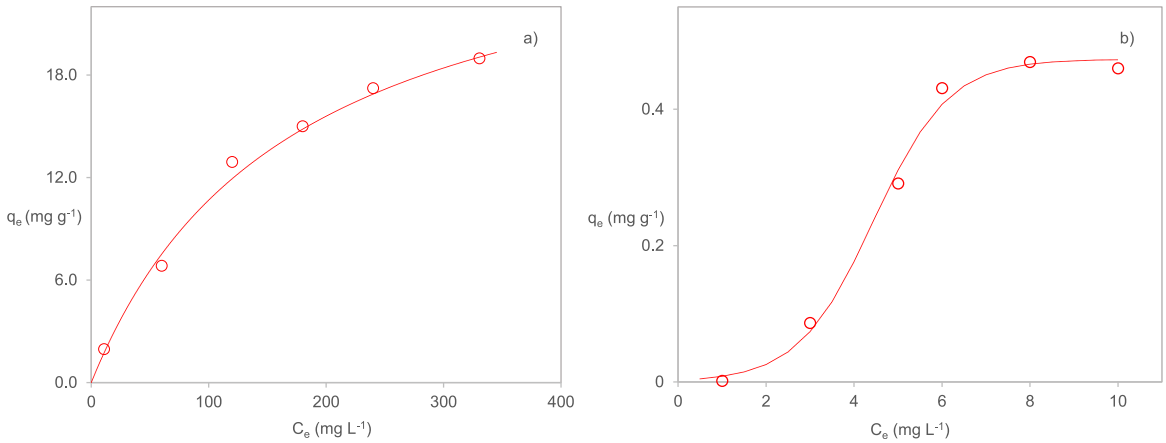

Fig. 5. Isotherm profiles of (a) OFL and (b) CORT on powders of GpB_46.

Table 2
Isotherm parameters obtained by fitting the experimental data of OFL and CORT.

		OFL	CORT
Langmuir	K_L (L mg^{-1})	0.006 ± 0.001	–
	q_{max} (mg g^{-1})	29 ± 2	–
	Reduced Chi-SQR	0.3604	–
	Adj. R-Square	0.9916	
Sigmoidal	A	–	1.2 ± 2
	F	–	4.4 ± 0.2
	q_{max} (mg g^{-1})	–	0.47 ± 0.02
	Reduced Chi-SQR	–	0.00044
	Adj. R-Square	–	0.9892

These results confirm a different drug adsorption mechanism: monolayer adsorption occurs on the geopolymer until OFL occupies all active sites, whereas CORT uptake is low at low CORT concentration and increases as the drug concentration increases. Previous studies have already demonstrated both adsorption mechanisms of OFL and other organic molecules on different aluminosilicates, natural, modified, and prepared from waste (Barreca et al., 2014; Belviso et al., 2021; Capsoni et al., 2022; Maraschi et al., 2014; Rivagli et al., 2014; Sturini et al., 2016). According to the models used, the calculated maximum adsorption capacities of pulverized GpB_46 are 29(2) mg g^{-1} for OFL and 0.47 (2) mg g^{-1} for CORT, which is in agreement with the experimental values. (See Table 2)

3.3. Drugs adsorption on porous monoliths and on a composite ceramic diaphragm

Based on promising results obtained under relevant realistic conditions, exploratory experiments were carried out with GpB_46_HP1, GpB_46_HP3, and GpB_46_O in their monolithic form. Each monolith was placed in 100 mL of tap water samples spiked with 10 mg L^{-1} OFL and CORT, each separately, under stirring. After 24 h of contact, the residual amount of OFL and CORT in the solution was determined by UV–Vis spectrophotometer and HPLC-UV, respectively.

These results, shown in Table 3, confirm the greater affinity of the geopolymer, both in powdered and porous monolith form, for the zwitterionic specie. Comparison between GpB_46_HP3 and GpB_46_HP1 shows that GpB_46_HP3 OFL removal capacity is twice that of GpB_46_HP1, consistent with the effective porosity of the two samples. As reported in Table 1, the effective porosity of GpB_46_HP3 is twice as large as that of GpB_46_HP1. Although GpB_46_O and GpB_46_HP1 showed similar porosity values, GpB_46_O achieved a quantitative OFL adsorption (> 95%) compared to GpB_46_HP1. This may be due to the different morphology. GpB_46_O is characterized by the presence of many fine and widespread pores. Instead, the pores in GpB_46_HP1 are larger and isolated resulting in a not too different total effective porosity but a smaller surface area. Concerning CORT, the adsorption is relatively poor and not significantly different for all the geopolymer samples considered, but still sufficient considering the environmental drug concentrations.

Finally, a ceramic composite diaphragm was tested in tap water (50 mL) enriched with 5 g L^{-1} OFL, the drug for which these geopolymers have shown a higher affinity. After 24 h of contact, a quantitative removal of OFL (> 99%) was observed.

Table 3
OFL and CORT adsorption on porous monoliths GpB_46_O, GpB_46_HP1 and GpB_46_HP3.

	Solution pH	OFL ads (%)	CORT ads (%)
GpB_46_O	6.0–6.4	95	8
GpB_46_HP1	6.0–6.4	43	12
GpB_46_HP3	6.0–6.4	86	14

3.4. Comparison with other kaolinite-based materials for FQs adsorption

The transformation of kaolinite into metakaolinite-based geopolymer significantly improves its adsorption capacity, and consequently its removal efficiency, especially towards OFL, as shown in Table 4.

The comparison among the pulverized kaolinite-based materials shows that the adsorption of ofloxacin on unmodified kaolinite ranges from 3.2 mg g^{-1} (Ma and Erping Bi, 2023) to 9 mg g^{-1} (Rivagli et al., 2014). Humic acid-kaolinite systems (Ma et al., 2023; Li et al., 2019) give comparable OFL adsorption capacities under similar experimental conditions. Only the novel composite material K-TAFe, synthesized by adding organic additives and iron cations, improves the OFL uptake significantly up to 137 mg g^{-1} (Chang et al., 2022). On the contrary, ionic liquids suppressed levofloxacin (LEV) uptake to 5 mg g^{-1} (Chen et al., 2023). Our work indicates that OFL adsorption on geopolymer powder is as high as 32 mg g^{-1} under relevant environmental conditions, encouraging its use for environmental applications. Moreover, it is competitive in FQs removal compared to a metakaolin/sludge-based geopolymer, ineffective alone, and quite efficient with incorporated hydroxyapatite and in the presence of copper cations for ciprofloxacin (CIP) adsorption (26 mg g^{-1}) (Arokiasamy et al., 2024).

4. Conclusions

In this paper, the adsorption properties of metakaolin-based geopolymers in the form of powders, porous monoliths, and a composite ceramic diaphragm for the removal from water of two CEC, namely, a fluoroquinolone antibiotic, ofloxacin (OFL), and a steroid hormone, cortisone (CORT) were investigated. The experimental results showed that geopolymers as such and in their foamed form have a greater affinity for OFL than CORT, especially below pH 6.5. The adsorption mechanism is quite different; monolayer adsorption occurs for OFL, whereas a cooperative adsorption is observed for CORT. Despite the significantly different adsorption capacities, under representative realistic conditions (freshwater and μg L^{-1} drugs) geopolymer powders gained quantitative adsorption of such persistent contaminants. Tests on porous monoliths and on a composite ceramic diaphragm were satisfactory for the removal of ofloxacin antibiotic, under the same experimental conditions.

CRediT authorship contribution statement

Serena C. Tarantino: Writing – original draft, Visualization, Resources, Project administration, Methodology, Funding acquisition,

Table 4
Adsorption capacity of various kaolinite-based materials. Other relevant experimental parameters were included for comparison.

FQ	Sorbent	Adsorption capacity (mg g^{-1})	Matrix	pH	Reference
CIP	GMK25S1-2Hap, 150 mg	26	distilled water	5–7	Arokiasamy et al., 2024
OFL	HA-K, 100 mg	5–7	0.01 M NaCl	5, 7, 9	Ma and Erping Bi, 2023
LEV	IL-K, 15 mg	5	0.01 M NaCl	5, 7, 9	Chen et al., 2023
OFL	K-TAFe, 10 mg	146	distilled water	6	Chang et al., 2022
OFL	DHA-K, 100 mg	0.5–6	NaCl 0.01 M	4.5,7,9.5	Li et al., 2019
OFL	K, 50 mg	9	tap water	2, 7.5	Rivagli et al., 2014
OFL	GpB_46, 50 mg	32	tap water	6	This work

Conceptualization. **Roberta Occhipinti:** Visualization, Investigation, Formal analysis. **Federica Maraschi:** Validation, Investigation. **Michele Zema:** Writing – review & editing, Methodology, Conceptualization. **M. Pia Riccardi:** Resources, Investigation. **Antonella Profumo:** Writing – review & editing, Resources, Methodology. **Michela Sturini:** Writing – original draft, Visualization, Methodology, Investigation, Formal analysis, Conceptualization.

Declaration of competing interest

The authors declare that they have no known competing financial interests or personal relationships that could have appeared to influence the work reported in this paper.

Data availability

Data will be made available on request.

Acknowledgments

This research was co-funded by the European Union under the LIFE Program, grant number LIFE19 ENV IT 000165-LIFE FREEDOM. RO was supported by Ministero dell'Istruzione, dell'Università e della Ricerca scholarship (Fondo per il sostegno dei giovani).

The authors wish to thank the suppliers of the materials utilized for the present work: Sibelco Italia S.p.A. (Sl kaolin) and Ingessil s.r.l. (waterglass). Dr. Stefano Puccia and Dr. Carlo Castiglioni are kindly acknowledged for their experimental support. Prof. Massimo Setti is thanked for his assistance with collecting XRPD patterns.

Appendix A. Supplementary data

Supplementary data to this article can be found online at https://doi.org/10.1016/j.clay.2024.107502.

References

Acisli, O., Acar, I., Khataee, A., 2020. Preparation of a fly ash-based geopolymer for removal of a cationic dye: isothermal, kinetic and thermodynamic studies. J. Ind. Eng. Chem. 83, 53–63. https://doi.org/10.1016/j.jiec.2019.11.012.

Acisli, O., Acar, I., Khataee, A., 2022. Preparation of a surface modified fly ash-based geopolymer for removal of an anionic dye: parameters and adsorption mechanism. Chemosphere 295, 133870. https://doi.org/10.1016/j.chemosphere.2022.133870.

Adeel, M., Song, X., Wang, Y., Francis, D., Yang, Y., 2017. Environmental impact of estrogens on human, animal and plant life: a critical review. Environ. Int. 99, 107–119. https://doi.org/10.1016/j.envint.2016.12.010.

Arokiasamy, P., Al Bakri Abdullah, M.M., Abd Rahim, S.Z., Sandu, A.V., Fedrigo, A., Ediati, R., Ishak, S., Kaus, N.H.M., 2024. Hydroxyapatite incorporated metakaolin/sludge based geopolymer adsorbent for copper ions and ciprofloxacin removal: Synthesis, characterization and mechanisms. Arab. J. Chem. 17, 105745 https://doi.org/10.1016/j.arabjc.2024.105745.

Babić, S., Horvat, A.J.M., Mutavdžić, Pavlović D., Kaštelan-Macan, M., 2007. Determination of pKa values of active pharmaceutical ingredients. TrAC 26, 1043–1061. https://doi.org/10.1016/j.trac.2007.09.004.

Bai, C., Franchin, G., Elsayed, H., Zaggia, A., Conte, L., Li, H., Colombo, P., 2017. High-porosity geopolymer foams with tailored porosity for thermal insulation and wastewater treatment. J. Mater. Res. 32, 3251–3259. https://doi.org/10.1557/jmr.2017.127.

Balan, E., Saitta, M.A., Mauri, F., Calas, G., 2001. First-principles modeling of the infrared spectrum of kaolinite. Am. Mineral. 86, 1321–1330. https://doi.org/10.2138/am-2001-11-1201.

Barreca, S., Orecchio, S., Pace, A., 2014. The effect of montmorillonite clay in alginate gel beads for polychlorinated biphenyl adsorption: isothermal and kinetic studies. Appl. Clay Sci. 99, 220–228. https://doi.org/10.1016/j.clay.2014.06.037.

Belviso, C., Guerra, G., Abdolrahimi, M., Peddis, D., Maraschi, F., Cavalcante, F., Ferretti, M., Martucci, A., Sturini, M., 2021. Efficiency in ofloxacin antibiotic water remediation by magnetic zeolites formed combining pure sources and wastes. Processes 9, 2137. https://doi.org/10.3390/pr9122137.

Capsoni, D., Lucini, P., Conti, D.M., Bianchi, M., Maraschi, F., De Felice, B., Bruni, G., Abdolrahimi, M., Peddis, D., Parolini, M., Pisani, S., Sturini, M., 2022. Fe_3O_4-halloysite nanotube composites as sustainable adsorbents: efficiency in ofloxacin removal from polluted waters and ecotoxicity. Nanomaterials 12, 4330. https://doi.org/10.3390/nano12234330.

Carvalheiras, J., Novais, R.M., Labrincha, J.A., 2023. Metakaolin/red mud-derived geopolymer monoliths: novel bulk-type sorbents for lead removal from wastewaters. Appl. Clay Sci. 106770 https://doi.org/10.1016/j.clay.2022.106770.

Castiglioni, S., Davoli, E., Riva, F., Palmiotto, M., Camporini, P., Manenti, A., Zuccato, E., 2018. Mass balance of emerging contaminants in the water cycle of a highly urbanized and industrialized area of Italy. Water Res. 131, 287–298. https://doi.org/10.1016/j.watres.2017.12.047.

Castiglioni, S., Zuccato, E., Fattore, E., Riva, F., Terzaghi, E., Koenig, R., Principi, P., Di Guardo, A., 2020. Micropollutants in Lake Como water in the context of circular economy: a snapshot of water cycle contamination in a changing pollution scenario. J. Hazard. Mater. 384, 121441 https://doi.org/10.1016/j.jhazmat.2019.121441.

Chang, Q., Gao, B., Yang, H., 2022. Efficient removal of fluoroquinolones antibiotics by using kaolin-tannic acid-Fe(III) composite adsorbents from water. Appl. Clay Sci. 222, 106490 https://doi.org/10.1016/j.clay.2022.106490.

Chen, J., Xu, B., Lu, L., Zhang, Q., Lu, T., Farooq, U., Chen, W., Zhou, Q., Qi, Z., 2023. Insight into the inhibitory roles of ionic liquids in the adsorption of levofloxacin onto clay minerals. Colloids Surf. A Physicochem. Eng. Asp. 666, 131303 https://doi.org/10.1016/j.colsurfa.2023.131303.

Clausi, M., Tarantino, S.C., Magnani, L.L., Riccardi, M.P., Tedeschi, C., Zema, M., 2016. Metakaolin as a precursor of materials for applications in Cultural Heritage: geopolymer-based mortars with ornamental stone aggregates. Appl. Clay Sci. 132–133, 589–599. https://doi.org/10.1016/j.clay.2016.08.009.

Duan, P., Yan, C., Zhou, W., Ren, D., 2016. Development of fly ash and iron ore tailing based porous geopolymer for removal of Cu(II) from wastewater. Ceram. Int. 42, 13507–13518. https://doi.org/10.1016/j.ceramint.2016.05.143.

Ducman, V., Korat, L., 2016. Characterization of geopolymer fly-ash based foams obtained with the addition of Al powder or H_2O_2 as foaming agents. Mater. Charact. 113, 207–213. https://doi.org/10.1016/j.jclepro.2021.127085.

Duxson, P., Provis, J.L., Lukey, G.C., Mallicoar, S.W., Kriven, W.M., van Deventer, J.S.J., 2005. Understanding the relationship between geopolymer composition, microstructure and mechanical properties. Colloids Surfaces A: Physicochem. Eng. Aspects 269, 47–58. https://doi.org/10.1016/j.colsurfa.2005.06.060.

En-naji, S., Ghazi, S., Mabroum, H., Mabroum, S., Khatib, K., Taha, Y., García Lodeiro, I., Hakkou, R., 2023. Design of acid-geopolymers based on clays by-products for methylene blue removal from wastewater. Appl. Clay Sci. 245, 107126 https://doi.org/10.1016/j.clay.2023.107126.

European Commission, Directorate-General for Environment, 2019. European Union Strategic Approach to Pharmaceuticals in the Environment. Communication from the Commission to the European Parliament, the Council and the European Economic and Social Committee, Document 52019DC0128, Brussels, Belgium. https://eur-lex.europa.eu/legal-content/en/ALL/?uri=CELEX%3A52019DC0128.

Farmer, V.C., 1998. Differing effect of particle size and shape in the infrared and Raman spectra of kaolinite. Clay Miner. 33, 601–6014. https://doi.org/10.1180/000985598545921.

Fletcher, R.A., MacKenzie, K.J.D., Nicholson, C.L., Shimada, S., 2005. The composition range of aluminosilicate geopolymers. J. Eur. Ceram. Soc. 25, 1471–1477. https://doi.org/10.1016/j.jeurceramsoc.2004.06.001.

Foo, K.Y., Hameed, B.H., 2010. Insights into the modeling of adsorption isotherm systems. J. Chem. Eng. 156, 2–10. https://doi.org/10.1016/j.cej.2009.09.013.

Gago-Ferrero, P., Bletsou, A.A., Damalas, D.E., Aalizadeh, R., Alygizakis, N.A., Singer, H. P., Hollender, J., Thomaidis, N.S., 2020. Wide-scope target screening of >2000 emerging contaminants in wastewater samples with UPLC-Q-ToF-HRMS/MS and smart evaluation of its performance through the validation of 195 selected representative analytes. J. Hazard. Mater. 387, 121712 https://doi.org/10.1016/j.jhazmat.2019.121712.

Gasparini, E., Tarantino, S.C., Ghigna, P., Riccardi, M.P., Cedillo-González, E.I., Siligardi, C., Zema, M., 2013. Thermal dehydroxylation of kaolinite under isothermal conditions. Appl. Clay Sci. 80-81, 417–425. https://doi.org/10.1016/j.clay.2013.07.017.

Gasparini, E., Tarantino, S.C., Conti, M., Biesuz, R., Ghigna, P., Ferdinando, A., Riccardi, M.P., Zema, M., 2015. Geopolymers from low-T activated kaolin: implications for the use of alunite-bearing raw materials. Appl. Clay Sci. 114, 530–539. https://doi.org/10.1016/j.clay.2015.06.040.

Gomez Cortes, L., Marinov, D., Sanseverino, I., Navarro Cuenca, A., Niegowska Conforti, M., Porcel Rodriguez, E., Stefanelli, F., Lettieri, T., 2022. Selection of Substances for the 4th Watch List under the Water Framework Directive. Publications Office of the European Union. https://doi.org/10.2760/909608.

Hossain, N., Bhuiyan, M.A., Pramanik, B.K., Nizamuddin, S., Griffin, G., 2020. Waste materials for wastewater treatment and waste adsorbents for biofuel and cement supplement applications: a critical review. J. Clean. Prod. 255, 120261 https://doi.org/10.1016/j.jclepro.2020.120261.

Iravani, R., An, C., Adamian, Y., Mohammadi, M., 2022. A review on the use of nanoclay adsorbents in environmental pollution control. Water Air Soil Pollut. 233, 109. https://doi.org/10.1007/s11270-022-05580-2.

Kümmerer, K., 2004. Resistance in the environment. J. Antimicrob. Chemother. 54, 311–320. https://doi.org/10.1093/jac/dkh325.

Li, Y., Bi, E., Chen, H., 2019. Effects of dissolved humic acid on fluoroquinolones sorption and retention to kaolinite. Ecotoxicol. Environ. Saf. 178, 43–50. https://doi.org/10.1016/j.ecoenv.2019.04.002.

Liao, M., Kelley, S., Yao, Y., 2020. Generating energy and greenhouse gas inventory data of activated carbon production using machine learning and kinetic based process simulation. ACS Sustain. Chem. Eng. 8, 1252–1261. https://doi.org/10.1021/acssuschemeng.9b06522.

Ma, C., Erping Bi, E., 2023. Active binding sites for ofloxacin resulted from adsorptive fractionation of humic acid on kaolinite. J. Environ. Manag. 325, 116473 https://doi.org/10.1016/j.jenvman.2022.116473.

Maleki, A., Hajizadeh, Z., Sharifi, V., Emdadi, Z., 2019. A green, porous and eco-friendly magnetic geopolymer adsorbent for heavy metals removal from aqueous solutions. J. Clean. Prod. 215, 1233–1245. https://doi.org/10.1016/j.jclepro.2019.01.084.

Mangla, D., Annu, Sharma, A., Ikram, S., 2022. Critical review on adsorptive removal of antibiotics: present situation, challenges and future perspective. J. Hazard. Mater. 425, 127946 https://doi.org/10.1016/j.jhazmat.2021.127946.

Maraschi, F., Sturini, M., Speltini, A., Pretali, L., Profumo, A., Pastorello, A., Kumar, V., Ferretti, M., Caratto, V., 2014. TiO_2-modified zeolites for fluoroquinolones removal from wastewaters and reuse after solar light regeneration. J. Environ. Chem. Eng. 2, 2170–2176. https://doi.org/10.1016/j.jece.2014.08.009.

Novais, R.M., Buruberri, L.H., Seabra, M.P., Labrincha, J.A., 2016. Novel porous fly-ash containing geopolymer monoliths for lead adsorption from wastewaters. J. Hazard. Mater. 318, 631–640. https://doi.org/10.1016/j.jhazmat.2016.07.059.

Novais, R.M., Carvalheiras, J., Tobaldi, D.M., Seabra, M.P., Pullar, R.C., Labrincha, J.A., 2019. Synthesis of porous biomass fly ash-based geopolymer spheres for efficient removal of methylene blue from wastewaters. J. Clean. Prod. 207, 350–362. https://doi.org/10.1016/j.jclepro.2018.09.265.

Novais, R.M., Pullar, R.C., Labrincha, J.A., 2020. Geopolymer foams: an overview of recent advancements. Prog. Mater. Sci. 109, 100621 https://doi.org/10.1016/j.pmatsci.2019.100621.

Nurlina, N., Hermayanti Pratama, J., Bagus Pambudi, A., Rahmawati, Z., Subaer, S., Al Bakri Abdullah, M.M., Gusrizal, G., Fansuri, H., 2024. A review of geopolymer membrane for water treatment. Appl. Clay Sci. 251, 107301 https://doi.org/10.1016/j.clay.2024.107301.

Pacheco-Torgal, F., Labrincha, J., Leonelli, C., Palomo, A., Chindaprasit, P., 2014. Handbook of Alkali-Activated Cements, Mortars and Concretes. Woodhead Publishing. ISBN: 9781782422761.

Papa, E., Minelli, M., Marchioni, M.C., Landi, E., Miccio, F., Natali Murri, A., Benito, P., Vaccari, A., Medri, V., 2023. Metakaolin-based geopolymer – Zeolite NaA composites as CO_2 adsorbents. Appl. Clay Sci. 237, 106900 https://doi.org/10.1016/j.clay.2023.106900.

Petlitckaia, S., Barré, Y., Piallat, T., Grauby, O., Ferry, D., Poulesquen, A., 2020. Functionalized geopolymer foams for cesium removal from liquid nuclear waste. J. Clean. Prod. 269, 122400 https://doi.org/10.1016/j.jclepro.2020.122400.

Pretali, L., Albini, A., Cantalupi, A., Maraschi, F., Nicolis, S., Sturini, M., 2021. TiO_2-photocatalyzed water depollution, a strong, yet selective depollution method: new evidence from the solar light induced degradation of glucocorticoids in freshwaters. Appl. Sci. 11, 2486. https://doi.org/10.3390/app11062486.

Provis, J.L., Palomo, A., 2015. Advances in understanding alkali-activated materials. Cem. Concr. Res. 78, 110–125. https://doi.org/10.1016/j.cemconres.2015.04.013.

Riva, F., Zuccato, E., Davoli, E., Fattore, E., Castiglioni, S., 2019. Risk assessment of a mixture of emerging contaminants in surface water in a highly urbanized area in Italy. J. Hazard. Mater. 361, 103–110. https://doi.org/10.1016/j.jhazmat.2018.07.099.

Rivagli, E., Pastorello, A., Sturini, M., Maraschi, F., Speltini, A., Zampori, L., Setti, M., Malavasi, L., Profumo, A., 2014. Clay minerals for adsorption of veterinary FQs: behavior and modelling. J. Environ. Chem. Eng. 2, 738–744. https://doi.org/10.1016/j.jece.2013.11.017.

Rovnanik, P., 2010. Effect of curing temperature on the development of hard structure of metakaolin-based geopolymer. Constr. Build. Mater. 24, 1176–1183. https://doi.org/10.1016/j.conbuildmat.2009.12.023.

Sahoo, S., Chakraborti, C.K., Mishra, S.C., Nathnanda, U., Naik, S., 2011. FTIR and XRD investigations of some fluoroquinolones. Int J Pharm Pharm Sci 3, 165–170.

Salimkhani, S., Siahcheshm, K., Kadkhodaie, A., Salimkhani, H., 2021. Structural analysis and the effect of the chromium on (Na) zeolite synthesized from kaolin. Mater. Chem. Phys. 271, 124957 https://doi.org/10.1016/j.matchemphys.2021.124957.

Sanguanpak, S., Wannagon, A., Saengam, C., Chiemchaisri, W., Chiemchaisri, C., 2021. Porous metakaolin-based geopolymer granules for removal of ammonium in aqueous solution and anaerobically pretreated piggery wastewater. J. Clean. Prod. 297, 126643 https://doi.org/10.1016/j.jclepro.2021.126643.

Sanguanpak, S., Shongkittikul, W., Saengam, C., Chiemchaisri, W., Chiemchaisri, C., 2022. TiO_2-immobilized porous geopolymer composite membrane for removal of antibiotics in hospital wastewater. Chemosphere 307, 135760. https://doi.org/10.1016/j.chemosphere.2022.135760.

Shahid, M.K., Kashif, A., Fuwad, A., Choi, Y., 2021. Current advances in treatment technologies for removal of emerging contaminants from water – a critical review. Coord. Chem. Rev. 442, 213993 https://doi.org/10.1016/j.ccr.2021.213993.

Shi, C., Qu, B., Provis, J.L., 2019. Recent progress in low-carbon binders. Cem. Concr. Res. 122, 227–250. https://doi.org/10.1016/j.cemconres.2019.05.009.

Sophia, A.C., Lima, E.C., 2018. Removal of emerging contaminants from the environment by adsorption. Ecotox. Environ. Safe. 150, 1–17. https://doi.org/10.1016/j.ecoenv.2017.12.026.

Sturini, M., Speltini, A., Maraschi, F., Profumo, A., Tarantino, S.C., Gualtieri, A.F., Zema, M., 2016. Removal of fluoroquinolone contaminants from environmental waters on sepiolite and its photo-induced regeneration. Chemosphere 150, 686–693. https://doi.org/10.1016/j.chemosphere.2015.12.127.

Syeed, M.M.M., Hossain, S., Karim, R., Uddin, M.F., Mahady Hasan, M., Razib Hayat Khan, R.H., 2023. Surface water quality profiling using the water quality index, pollution index and statistical methods: a critical review. Environ. Sustain. Indic. 18, 100247 https://doi.org/10.1016/j.indic.2023.100247.

Tan, T.H., Mo, K.H., Ling, T.C., Lai, S.H., 2020. Current development of geopolymer as alternative adsorbent for heavy metal removal. Environ. Technol. Innov. 18, 100684 https://doi.org/10.1016/j.eti.2020.100684.

Van Doorslaer, Xander, Dewulf, Jo, Van Langenhove, Herman, Demeestere, Kristof, 2014. Fluoroquinolone antibiotics: an emerging class of environmental micropollutants. Sci. Total Environ. 500-501, 250–269. https://doi.org/10.1016/j.scitotenv.2014.08.075.